Evidence for a Dynamic Structure of Human Neuronal Growth Inhibitory Factor and for Major Rearrangements of Its Metal−Thiolate Clusters†

Peter Faller,‡ Daniel W. Hasler,‡ Oliver Zerbe,§ Stefan Klauser,‡ Dennis R. Winge,|| and Milan Vašák*,‡

Institute of Biochemistry, University of Zürich, Winterthurerstrasse 190, CH-8057 Zürich, Switzerland, Department of Pharmacy, ETH, Winterthurerstrasse 190, CH-8057 Zürich, Switzerland, and Department of Biochemistry, University of Utah Health Science Center, Salt Lake City, Utah 84132

Received March 2, 1999; Revised Manuscript Received May 27, 1999

ABSTRACT: Human neuronal growth inhibitory factor (GIF), a metallothionein-like protein classified as metallothionein-3, impairs the survival and the neurite formation of cultured neurons. Despite its approximately 70% amino acid sequence identity with those of mammalian metallothioneins (MT-1 and MT-2 isoforms), only GIF exhibits growth inhibitory activity. In this study, structural features of the metal−thiolate clusters in recombinant Zn_7- and Cd_7-GIF, and in part also in synthetic GIF (68 amino acids), were investigated by using circular dichroism (CD) and ^{113}Cd NMR. The CD and ^{113}Cd NMR studies of recombinant Me_7-GIF confirmed the existence of distinct Me_4S_{11}- and Me_3S_9-clusters located in the α- and β-domains of the protein, respectively. Moreover, a mutual structural stabilization of both domains was demonstrated. The ^{113}Cd NMR studies of recombinant $^{113}Cd_7$-GIF were conducted at different magnetic fields (66.66 and 133.33 MHz) and temperatures (298 and 323 K). At 298 K the spectra revealed seven ^{113}Cd signals at 676, 664, 651, 644, 624, 622, and 595 ppm. A striking feature of all resonances is the absence of resolved homonuclear [$^{113}Cd-^{113}Cd$] couplings and large apparent line widths (between 140 and 350 Hz), which account for the absence of cross-peaks in [^{113}Cd, ^{113}Cd] COSY. On the basis of a close correspondence in chemical shift positions of the ^{113}Cd signals at 676, 624, 622, and 595 ppm with those obtained in our previous studies of $^{113}Cd_4$-GIF(32−68) [Hasler, D. W., Faller, P., and Vašák, M. (1998) *Biochemistry 37*, 14966], these resonances can be assigned to a Cd_4S_{11}-cluster in the α-domain of $^{113}Cd_7$-GIF. Consequently, the remaining three ^{113}Cd signals at 664, 651, and 644 ppm originate from a Me_3S_9 cluster in the β-domain. However, the latter resonances show a markedly reduced and temperature-independent intensity (∼20%) when compared with those of the α-domain, indicating that the majority of the signal intensity remained undetected. To account for the observed NMR features of $^{113}Cd_7$-GIF, we suggest that dynamic processes acting on two different NMR time scales are present: (i) fast exchange processes among conformational cluster substates giving rise to broad, weight-averaged resonances and (ii) additional very slow exchange processes within the β-domain associated with the formation of configurational cluster substates. The implications of the structure fluctuation for the biological activity of GIF are discussed.

Alzheimer's disease (AD)[1] is characterized by extensive neurodegeneration accompanied by the formation of neurofibrillary tangles and amyloid plaques (*1*). Uchida et al. (*2*) discovered that AD brain extract increased rat cortical neuron survival and neuronal sprouting in vitro more effectively than brain extract of normal human brains, suggesting the presence of elevated neurotrophic activity in AD brain. This apparent increase in neurotrophic activity was found to be due to the loss of a growth inhibitory factor (GIF), which was subsequently isolated from normal human brains (*3*). Following studies have confirmed the growth inhibitory activity of this protein but its deficiency in AD brains has been put in question (*4*). However, in recent immunohistochemical studies of the brains of patients with Down syndrome, characterized by an AD type of pathology, the loss of GIF in astrocytes around senile plaques has been demonstrated (*5*).

The characterization of GIF revealed a metalloprotein of 68 amino acids containing four copper and three zinc ions (*3*). The amino acid sequence of human GIF exhibits about 70% sequence identity with those of mammalian metallothioneins (MTs, 61 amino acids), including the preserved array of 20 cysteines (*3*). Similar amino acid sequences have also been reported for GIF from various mammalian species

† This work was supported in part by Swiss National Science Foundation Grant 32-49460.96, Stipendienfonds der Basler Chemischen Industrie (D.W.H) and EMDO Stiftung (P.F.).

* To whom correspondence should be addressed. Phone: (+41)-1-635 5552. Fax: (+41)-1-635 6805.

‡ University of Zürich.

§ ETH.

|| University of Utah Health Science Center.

[1] Abbreviations: AD, Alzheimer's disease; CD, circular dichroism; CSA, chemical shift anisotropy; ESI-MS, electrospray ionization mass spectrometry; EXAFS, extended X-ray absorption fine structure; DTT, 1,4-dithiothreitol (*threo*-1,4-dimercapto-2,3-butanediol); GIF, growth inhibitory factor; GIF(1−32), N-terminal domain of GIF (amino acid residues 1−32); GIF(32−68), C-terminal domain of GIF (amino acid residues 32−68); IPTG, isopropyl-β-D-thiogalactopyranoside; LBB, Luria Broth Base (Miller's LB Broth Base); LMCT, ligand-to-metal charge transfer; MBB, monobromobimane (*syn*-3-brommethyl-2,4-dimethyl[1,5-diazabicyclo[3.3.0]octadienone]); MT, metallothionein; TED-buffer, Tris/EDTA/DTT buffer.

10.1021/bi990489c CCC: $18.00
Published on Web 07/09/1999

(*6*−*10*). Relative to the amino acid sequences of mammalian MTs (MT-1, MT-2 isoforms), the consensus GIF sequence contains two inserts, a single Thr in the N-terminal region and a Glu-rich hexapeptide in the C-terminal region. In addition, two conserved proline residues are present in the Cys(6)-Pro-Cys-Pro(9) motif. Molecular biological studies revealed that the GIF gene has a similar size, shares intron/exon boundaries, and is clustered on the same chromosome as MTs. These features led to its classification as MT-3 (*6*, *11*).

Despite high similarities between the primary structures of GIF and mammalian MTs, the biological properties of these proteins differ remarkably. Thus, in contrast to mammalian MTs, which are expressed in most organs and are believed to play a role in the homeostasis of the essential trace metals (Zn, Cu) and in the heavy metal detoxification (Cd, Hg) (*12*−*14*), human GIF is expressed almost exclusively in the brain (*15*). Moreover, only GIF but not MTs could be shown to exhibit growth inhibitory activity in neuronal cell culture studies (*3*, *4*). To test the tissue specific effect of GIF, transgenic mice that expressed GIF using control elements from the MT-1 locus were compared with those in which extra MT-1 was expressed under the same regulation (*16*). Transgenic mice expressing excess MT-1 did not show any pathological effects. However, those with ectopical GIF expression died at 2 months of age with the pathological characteristics of pancreatic acinar cell necrosis and fibrosis. This result provides further evidence for the distinct biological and structural properties of this protein.

In contrast to mammalian MTs, which usually contain seven Zn(II) ions, isolated human GIF contains an unusual metal composition of four copper and three zinc (*3*). A similar metal composition has also been found in GIF isolated from bovine brain (*7*) and its growth inhibitory activity has been confirmed using a new neuronal assay (*17*). Spectroscopic studies on bovine Cu,Zn-GIF showed that the Cu(I) and Zn(II) ions are organized into two independent homometallic metal−thiolate clusters (*18*, *19*). However, the localization of these clusters within the protein structure is currently not known.

Other studies compared the growth inhibitory activity of recombinant and metal-reconstituted human GIF containing seven Zn(II) ions, with those of the individual α-domain, GIF(32−68), and the β-domain, GIF(1−32), reconstituted with four and three Zn(II) ions, respectively. The recombinant Zn_7-GIF and Zn_3-GIF(1−32) exhibited the same degree of growth inhibitory activity, whereas Zn_4-GIF(32−68) possessed no activity (*20*). Independently, using a limited protease digestion of human GIF, the growth inhibitory activity of the isolated β-domain (amino acids 1−26) has also been demonstrated (*21*). Further studies by Sewell et al. (*20*) revealed that the growth inhibitory activity of human Zn_3-GIF(1−32) is abolished by the mutation of the Cys(6)-Pro-Cys-Pro(9) sequence either to Cys-Ser-Cys-Ala or to Cys-Thr-Cys-Thr. The former mutation represents the amino acid sequence found in human MT-1/MT-2 (*12*).

Metal−thiolate clusters formed with the divalent (Zn^{II}, Cd^{II}) and monovalent (Cu^{I}) ions in both separated GIF domains were studied by spectroscopy. In the case of the biologically active β-domain, distinct $Me^{II}_3S_9$-, Cu_4S_{8-9}-, and Cu_6S_9-clusters have been formed with widely different spectroscopic properties compared with similar clusters in the individual β-domain of mammalian MTs (*22*). This conclusion has been supported by the subsequent Zn K-edge EXAFS studies of Zn_3-GIF(1−32) and Zn_7-GIF (*19*). However, a large conformational flexibility within the Zn_3- and Cd_3-GIF(1−32) domain precluded their detailed investigations by NMR (*22*). Similar spectroscopic studies using GIF-(32−68) established the formation of $Me^{II}_4S_{11}$-, Cu_4S_{8-9}-, and Cu_6S_{11}-clusters. However, in contrast to the ^{113}Cd NMR studies of the isolated $^{113}Cd_4$-α-domain of MT, the ^{113}Cd NMR characterization of $^{113}Cd_4$-GIF(32−68) revealed all four ^{113}Cd signals only at elevated temperature (323 K), indicating the presence of a large conformational flexibility also in this GIF domain. (*23*). Thus, although metal clusters with divalent metal ions reveal similar metal/thiolate stoichiometries for both GIF and mammalian MTs, the structure of GIF has to differ substantially from the established three-dimensional structure of mammalian Me^{II}_7-MTs (*24*).

The aim of the present study was to examine the metal organization and conformational flexibility of both GIF domains in the entire protein. The structural features of recombinant human Zn_7- and Cd_7-GIF have been investigated by circular dichroism (CD) and that of $^{113}Cd_7$-GIF by ^{113}Cd NMR. The results are compared with those obtained previously for the isolated GIF domains (*22*, *23*). In addition, a detailed account of the optimization of GIF expression and protein purification is reported. Furthermore, the total solid-phase synthesis of GIF—the first for a mammalian MT—as an alternative source of GIF is discussed.

MATERIALS AND METHODS

GIF Expression. Transformed *Escherichia coli* BL21-(pLysS) containing human GIF cDNA on a pET3d expression vector (Novagen) was used for expression as described previously (*4*). Fresh LBB cell culture medium was inoculated with 1% (v/v) of an overnight preculture containing ampicillin (50 μg/L) and chloramphenicol (34 μg/L) and was subsequently grown to an OD_{600} of 0.5−0.6. Expression of GIF was induced by adding 0.4 mM IPTG (0.8 mL of a 0.5 M IPTG solution/L of culture). After 30 min of further growth, 0.3 mM Zn(II) (0.3 mL of a 1 M $ZnCl_2$ solution/L of culture) was added. The *E. coli* culture growth was continued for another 2.5−3.0 h. The cells were pelleted by centrifugation (20 min at 4 °C and 4000*g*), and then resuspended in 10 mL of buffer (50 mM Tris/HCl, 100 mM NaCl, 60 mM 2-mercaptoethanol, pH 8.0) per liter of culture medium and stored overnight at −70 °C.

Purification of Recombinant GIF. The frozen cell pellet prepared from a total of 6 L of culture medium was thawed, and the volume increased 5-fold using the same buffer (see above) and sonicated for 5 min on ice. To this suspension, an equal volume of chilled (−20 °C) ethanol/chloroform mixture (97:3 v/v) was slowly added. The resulting precipitate was removed by centrifugation at 18000*g* for 20 min at 4 °C. Subsequently, 3 vol of ethanol (−20 °C) was slowly added to the supernatant on ice, and the resultant suspension was allowed to sediment out overnight at −20 °C. The supernatant was decanted and the remaining suspension centrifuged at 25000*g* for 30 min. The pellet was dissolved in 8 mL of buffer (50 mM Tris/HCl, 100 mM NaCl, and 5 mM 2-mercaptoethanol, pH 8.0). After a 15 min incubation of the suspension with 1 mg of bovine pancreatic DNase I

(Boehringer Mannheim, grade II) at room temperature, the 2-mercaptoethanol concentration was increased to 60 mM. The sample was centrifuged, and the supernatant was loaded onto a gel filtration column (Superdex-75 HiLoad 26/60 FPLC column, Pharmacia) equilibrated with 25 mM Tris/HCl and 50 mM NaCl at pH 8.0. The protein was eluted with the same buffer. The protein fractions were monitored at 290 nm and their zinc content was determined by atomic absorption spectrometry (IL Video 12). The Zn-containing peak at an apparent molecular mass of approximately 20 kDa was pooled and concentrated by ultrafiltration (Amicon, YM1 membrane). The GIF sample was adsorbed on a DEAE MemSep-1500 cartridge (Millipore) attached to a FPLC system (Pharmacia) and eluted with a linear gradient of 0 to 200 mM NaCl in 10 mM Tris/HCl, pH 8.6, at a flow rate of 8 mL/min. The Zn-containing GIF fractions, which eluted at about 170 mM NaCl, were pooled. To examine the purity of GIF, a small aliquot of this sample was saturated with Ar (10 min), followed by a pH adjustment to 2 with 1 M HCl. The sample was applied to an analytical C_{18} reversed-phase HPLC column (Brownlee Aquapore ODS 300, 0.4 cm × 22 cm) equilibrated with 0.1% TFA. Elution was performed with a linear gradient from 0 to 60% buffer B (B = 0.1% TFA and 80% acetonitrile); GIF eluted at about 35% acetonitrile. Mass spectrometry revealed a molecular mass of 6926.9 Da, which is in close agreement with the calculated mass of 6927.1 Da. In some instances, an additional HPLC peak was detected at about 31% acetonitrile. The ESI-MS of this sample (6924.9 Da) revealed a mass difference of 2 Da, suggesting the presence of an intramolecular disulfide bridge in this GIF fraction. The treatment of this sample with 2-mercaptoethanol or DTT prior to the pH adjustment for HPLC yielded the fully reduced form of GIF. The presence of 2-mercaptoethanol during the purification as described above leads in most cases to reduced GIF only (yield 3−4 mg/L).

In a few instances, Cd-GIF has also been prepared in the manner described above. However, as the preparation of this metalloform has been accompanied by additional difficulties, i.e., the presence of polymeric species (see below), only the preparation of the Zn-containing GIF form has been described.

Detection of the Recombinant GIF Expression. As the yield of expression may vary, the presence of a sufficient amount of GIF was routinely estimated prior to large-scale GIF purification. The amount of GIF in the cell pellet was checked by using either SDS−PAGE or absorption spectroscopy, the latter bearing the advantage of providing a better estimation of the GIF content. For both procedures, an aliquot of the resuspended cell pellet of the expression was dissolved in 300 μL of 50 mM Tris/HCl, 100 mM NaCl, and 60 mM 2-mercaptoethanol, pH 8.0, sonicated, and centrifuged prior to use (5 min, Eppendorf bench centrifuge).

(i) The sensitivity of GIF detection in SDS−PAGE can be dramatically enhanced by thiol modification with monobromobimane (MBB) and the product detected by fluorescence (*25*). A total of 10 μL of the supernatant of the sonicated cells was combined with 30 μL of TED buffer (20 mM Tris/HCl, 100 mM EDTA, and 2 mM DTT, pH 8.0) and 60 μL of monobromobimane (100 mM in acetonitrile). The mixture was incubated for 40 min at room temperature in the dark. Then 3 μL of 5× concentrated Laemmli sample buffer was added to 12 μL of the sample, heated for 5 min at 90 °C, and applied to SDS−PAGE (*26*). The MBB fluorescence of the proteins on gels was visualized using a transilluminator equipped with a 365 nm light source and photographed using a 460 nm long-pass emission filter in between.

(ii) The quantification of GIF by absorption spectroscopy was performed as follows: the supernatant of the sonicated cells was applied to a gel filtration column (Superdex-75 HR 10/30, Pharmacia) and equilibrated in 25 mM Tris/HCl and 50 mM NaCl, pH 8.0. Elution with the same buffer was monitored by the absorbance at 240 nm and by atomic absorption spectrometry. A major Zn-containing peak, eluting with an apparent molecular mass of approximately 20 kDa, showed features of GIF. To estimate the amount of Zn_7-GIF present, the replacement of the Zn(II) ions by Cd(II) and the development of the typical CysS−Cd(II) charge-transfer band at 250 nm was examined. For this purpose, the electronic absorption spectrum of the main Zn-fraction of the putative GIF peak has been measured. After adding an excess of $CdCl_2$, the spectrum was measured again. The Cd(II) ions replace the Zn(II) ions in GIF rapidly (<1 min). The Cd_7-GIF form showed the typical 250 nm shoulder from which the yield of GIF expression can be estimated using the extinction coefficient, $\epsilon_{250} = 100\,000\ M^{-1}\ cm^{-1}$ (*18*).

Total Solid-Phase Synthesis and Purification of Synthetic GIF. Synthetic human GIF (68 amino acids) was synthesized by standard F-moc chemistry on an ABI 433 A peptide synthesizer. The synthetic protein consisted of the following sequence: MDPETCPCPSGGSCTCADSCKCEGCKCTSCK-KSCCSCCPAECEKCAKDCVCKGGEAAEAEAEKCSCCQ. A 0.05 mmol peptide synthesis was carried out using conditions recommended by the manufacturer. The F-moc Lys(Boc)-Wang resin (p-benzyloxybenzyl resin) was used as the solid support. All amino acids were incorporated with 9-fluorenylmethoxycarbonyl (F-moc) at the α amino group, and the side-chain functional groups were protected as follows: O-*tert*-butylaspartic acids, O-*tert*-butylglutamic acid, O-*tert*-butylserine, O-*tert*-butylthreonine, *S*-tert-phenylcysteine, and lysine(Boc). All amino acids and the resin were products of Bachem, Switzerland. The cleavage of the synthesized peptide from the resin and the removal of the side-chain protecting groups was achieved by treatment with a solution containing 0.75 g of phenol, 0.25 mL of ethanediol, 0.5 mL of thioanisole, 0.5 mL of H_2O, and 10 mL of TFA. In a subsequent step, the peptide was precipitated with *tert*-butylmethyl ether. The synthetic GIF peptide was purified by dissolving the crude product in 10 mM HCl/5 M urea, desalting over a gel filtration column (G-10) followed by a C_{18} reverse-phase HPLC step on a semipreparative column (Brownlee, Aquapore ODS 300). For the further purification at neutral pH, synthetic GIF was reconstituted with Cd(II) according to Vašák 1991 (*27*) and desalted over a gel filtration column (Superdex-75 HR 10/30, Pharmacia) equilibrated in 25 mM Tris/HCl, 50 mM NaCl, pH 8.0. Synthetic Cd_7-GIF eluted with an apparent molecular mass of about 20 kDa. The sample was subsequently diluted 10 times with water and passed over an ion-exchange column (TDSK, TosoHaas, DEAE−5PW, 7.5 mm × 7.5 cm, 10 μm) with a linear gradient from 40 to 400 mM Tris/HCl, pH 7.5, in 30 min at a flow rate of 1 mL/min. The elution of synthetic Cd_7-GIF was monitored by the absorbance at 254 nm. The

main chromatographic peak at about 230 mM Tris/HCl has been analyzed for purity by using an analytical HPLC column (Brownlee Aquapore ODS 300). HPLC analysis revealed a symmetrical, sharp peak with the same retention time as found for recombinant GIF (for conditions see above). Electrospray mass spectrometry of this peak yielded a mass of 6926.7 Da for synthetic GIF. This value agrees closely with the calculated mass of 6927.1 Da.

Metal Reconstitution of GIF. The Cd forms of recombinant and synthetic GIF were generated by the method of Vašák (*27*). In brief, 8 equiv of $CdCl_2$ was added to N_2 saturated GIF solution (0.1 mg mL^{-1} protein in 10 mM HCl), followed by pH adjustment to 8.6 with 0.5 M Tris base (Fluka). To remove an excess of Cd(II) ions, a small amount of Chelex 100 resin (Bio-Rad) was added to the sample and the suspension incubated for 5 min. The Chelex 100 resin was removed by filtration. Alternatively, an excess of Cd(II) was removed by passing the sample through a gel filtration column (Superdex 75). The Zn-GIF forms were prepared in a similar manner. Metal-to-GIF ratios were determined using a small aliquot of the sample. The metal concentration was determined by atomic absorption spectrometry (IL Video 12) and that of the peptide via sulfhydryl concentration (20 Cys per peptide). In the latter case, the sulfhydryl reaction with 2,2′-dithiopyridine in 0.2 M sodium acetate and 1 mM EDTA (pH 4) was followed spectroscopically and the concentration determined using $\epsilon_{343} = 7600\ M^{-1}\ cm^{-1}$ (*28*).

Spectroscopic Measurements. Absorption spectra were recorded on a Cary 3 spectrometer. CD measurements were made using a Jasco (model J-715) spectropolarimeter. The CD spectra are expressed as a molar ellipticity, [θ] (deg $dmol^{-1}\ cm^{-1}$). ^{113}Cd NMR spectra were recorded on Bruker AMX-600 and/or AMX-300 spectrometers using inverse-gated broadband proton decoupling to account for possible negative $^{113}Cd,^{1}H$ NOE. Data were sampled over a 62 500 Hz spectral-width using a 0.13 s acquisition time. Experiments recorded with 0.4 and 2 s pulse-repetition rates showed very similar spectra and hence the shorter relaxation delay was used to obtain a better signal-to-noise ratio. All NMR samples contained 10% $^{2}H_2O$ for the field-frequency lock and were measured in 5 mm NMR tubes. The ^{113}Cd chemical shifts are given in parts per million relative to external standard 0.1 M $Cd(ClO_4)_2$.

RESULTS

Expression and Purification of Recombinant GIF. As described in the Materials and Methods, some important points have to be considered for successful expression and purification of recombinant GIF. First, in contrast to the expression of metallothioneins in *E. coli* cultures, it turned out to be advantageous to express GIF as the Zn- instead of the Cd-containing form. We observed that Cd_7-GIF tends to form higher molecular weight aggregates, complicating its purification. Second, the presence of 2-mercaptoethanol throughout the purification of Zn_7-GIF was beneficial since it apparently prevents protein oxidation and the formation of aggregates due to metal and/or disulfide bridges. Finally, increasing the volume of the suspended cells by dilution with a buffer prior to the sonication step also seemed to be important, as at smaller volumes, a lower protein yield was obtained. We ascribe this effect to a more efficient protein recovery from the putative inclusion bodies, well-known to contain disulfide bonds (*29*).

The commonly used Coomassie blue staining for proteins in SDS−PAGE gels was found to be insensitive for monitoring the content of GIF since no band enhancement between induced and noninduced *E. coli* cultures was detected. Independent checks using purified recombinant GIF established that this staining is only successful when a substantial amount of the protein is applied (approximately 5 μg). Therefore, two new detection methods for GIF were applied. To monitor GIF expression in *E. coli* cultures, a far more sensitive fluorescence staining method was used. The latter method is based on the modification of thiols with monobromobimane (MBB), followed by fluorescence detection of the product in SDS−PAGE. The detection relies on the fact that MTs have the highest cysteine content of all known proteins (~30%) and that unreacted MBB does not show any fluorescence under the conditions described in the Materials and Methods (*25*). To estimate the yield of GIF expression prior to a large-scale protein purification, a combination of small scale gel filtration chromatography and absorption spectroscopy was used. This method relies on the replacement of the more weakly bound Zn(II) ions in Zn_7-GIF by Cd(II). The absorption spectrum of the Zn-containing peak from the gel filtration was measured before and after adding Cd. The intensity of the induced shoulder at 250 nm, due to the CysS−Cd(II) LMCT transitions, was used to estimate the amount of GIF in the sample (see Materials and Methods).

Solid-Phase Synthesis of GIF. Solid-phase synthesis is a valuable source for peptides or small proteins and bears the potential to easily introduce specifically labeled amino acid(s) for structural and/or biological studies. Having successfully synthesized both domains of human GIF, the feasibility of this approach as an alternative source of GIF was also examined. Human GIF (68 amino acids) has been chemically synthesized by F-moc chemistry. This represents the first example of a total synthesis of mammalian MT. The protein can be purified by taking advantage of the pronounced physicochemical differences between apo-GIF and holo-GIF. In the first step, the predominantly random coil apo-protein was purified using semipreparative HPLC at low pH. The subsequent incorporation of seven Cd(II) ions into metal-free synthetic GIF allowed for a further purification of the synthetic Cd_7-GIF form, using conventional ion-exchange chromatography at neutral pH. Analytical RP-HPLC of purified synthetic GIF in TFA/acetonitrile revealed a single sharp peak with a retention time similar to that found for recombinant GIF, as would be expected for the pure protein. The presence of a single-mass peak of 6926.7 Da (calculated mass = 6927.1 Da) in the ESI-MS spectrum of metal-free GIF established the correctness of the synthesis. The Zn(II)- and Cd(II)-metal binding and the corresponding electronic absorption and CD features were found to be identical to those described below for recombinant GIF. However, the overall yield of the 0.05 mmol synthesis (300 mg of the crude peptide) is only about 2% and is thus comparable to that obtained for recombinant GIF from 1 to 2 L of cell culture. Thus, when no specific labeling is needed, recombinant GIF is less costly and the protein is purified faster than synthetic GIF and has therefore been used in further studies.

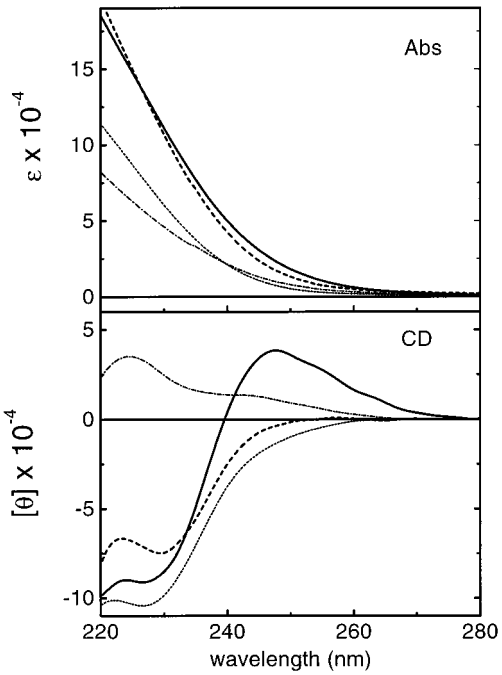

FIGURE 1: Electronic absorption (Abs) and circular dichroism (CD) spectra of Zn_7-GIF (—), Zn_3-GIF(1−32) (−•−), Zn_4-GIF(32−68) (---) and the sum of both domains (− − −) in 25 mM Tris/HCl and 50 mM NaCl, pH 8.0.

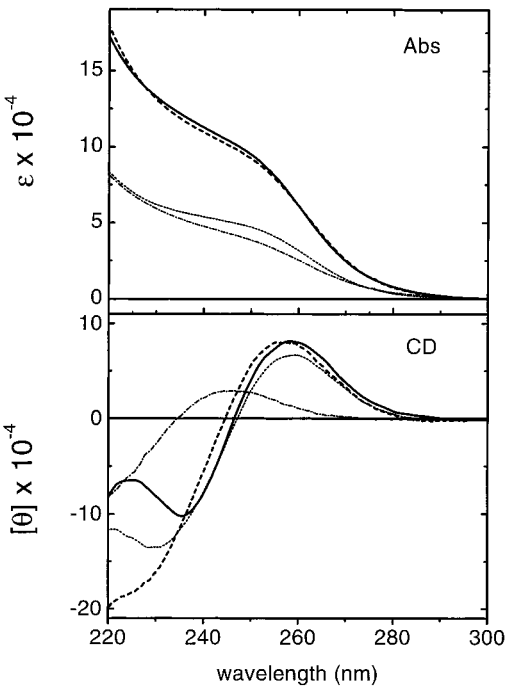

FIGURE 2: Electronic absorption (Abs) and circular dichroism (CD) spectra of Cd_7-GIF (—), Cd_3-GIF(1−32) (−•−), Cd_4-GIF(32−68) (- - -) and the sum of both domains (− − −) in 25 mM Tris/HCl and 50 mM NaCl, pH 8.0.

Electronic Absorption and CD Studies of Zn(II)- and Cd(II)-GIF Derivatives. To check the correct incorporation of the metals by in vitro reconstitution, the spectroscopic features of reconstituted GIF were compared with those of the directly isolated GIF from *E. coli* cultures. The reconstituted Cd(II)- and Zn(II)-GIF derivatives were generated as described above. For both metalloforms a metal/protein ratio of 7 ± 0.15 was obtained. Similar metal/protein ratios have also been found for Zn(II)- and Cd(II)-GIF isolated directly from *E. coli* cultures grown in the presence of Zn(II) and Cd(II) salts, respectively. The electronic absorption and CD spectra of directly isolated and reconstituted Zn(II)- and Cd(II)-GIF forms were found to be very similar, proving the correctness of the metal reincorporation. This result is especially crucial for ^{113}Cd NMR studies in which the ^{113}Cd reconstituted $^{113}Cd_7$-GIF is used.

Representative absorption and CD spectra of the Zn(II)- and Cd(II)-containing metalloforms are depicted in Figures 1 and 2, respectively (solid line). It should be noted that metal-free GIF, like mammalian MTs, does not show appreciable absorption above 220 nm, due to the absence of aromatic amino acids and histidine. The absorption spectrum of Zn_7-GIF is characterized by an unresolved tailing toward the high-energy region starting at about 270 nm (Figure 1). The corresponding CD spectrum is dominated by strong CD bands at (−)228 and (+)247 nm with a crossover point at 239 nm. These CD features are similar in shape to those reported for mammalian Zn_7-MT and can thus be assigned to CysS−Zn(II) LMCT transitions (*30*). However, in contrast to the CD profile of Zn_7-MT, characterized by bands at (+)242 and (−)228 nm with a crossover point at 233 nm, the low-energy region of the Zn_7-GIF spectrum is substantially red-shifted.

In the absorption spectrum of Cd_7-GIF, a characteristic shoulder at about 250 nm, commonly found in Cd-MT complexes, is discerned. By analogy to Cd-MTs, we assign the underlying bands to the CysS−Cd(II) LMCT transitions (*31*). The molar extinction coefficient of Cd_7-GIF at 250 nm (100 000 M^{-1} cm^{-1}) reveals a value of 5.0×10^3 M^{-1} cm^{-1} per CysS bound to a Cd(II). This value, which is similar to that reported for CysS−Cd bond in a number of Cd-substituted metalloproteins (*32*) and the fact that the absorption does not increase upon addition of an excess of Cd(II), strongly suggests that all 20 cysteines of the protein are involved in metal binding. The corresponding CD spectrum of Cd_7-GIF (Figure 2) exhibits a biphasic profile with a positive and negative extrema at (+)258 and (−)238 nm, respectively. Such a biphasic CD spectrum with bands at (+)258 and (−)239 nm was also found in mammalian Cd_7-MT and was assigned to an excitonic coupling of transition dipole moments located at the bridging thiolate ligands in the clusters (*33*).

^{113}Cd NMR Studies of $^{113}Cd_7$-GIF. In the structural studies of Cd-MTs, ^{113}Cd NMR proved to be indispensable to investigate the organization of metal-binding sites and [^{1}H,^{113}Cd] COSY allowed the direct identification of cysteine residues as the sole coordinating ligands (*34*). The ^{113}Cd NMR studies of recombinant $^{113}Cd_7$-GIF were conducted at 298 and 323 K and at the frequencies of 133.33 and 66.66 MHz (corresponding to 600 and 300 MHz proton frequencies, respectively). The 133 MHz ^{113}Cd NMR spectra of reconstituted human $^{113}Cd_7$-GIF and for comparison also of rabbit liver $^{113}Cd_7$-MT-2, are presented in Figure 3. It may be noted that the three-dimensional structure of rabbit liver $^{113}Cd_7$-MT has been solved by NMR (*35*). At 298 K, $^{113}Cd_7$-GIF shows seven ^{113}Cd signals at 676, 664, 651, 644, 624, 622, and 595 ppm corresponding to seven distinct metal-binding sites. The chemical shift position of all resonances, except for that at 595 ppm, are very similar to those reported for mammalian $^{113}Cd_7$-MTs (*35*−*39*), suggesting that the

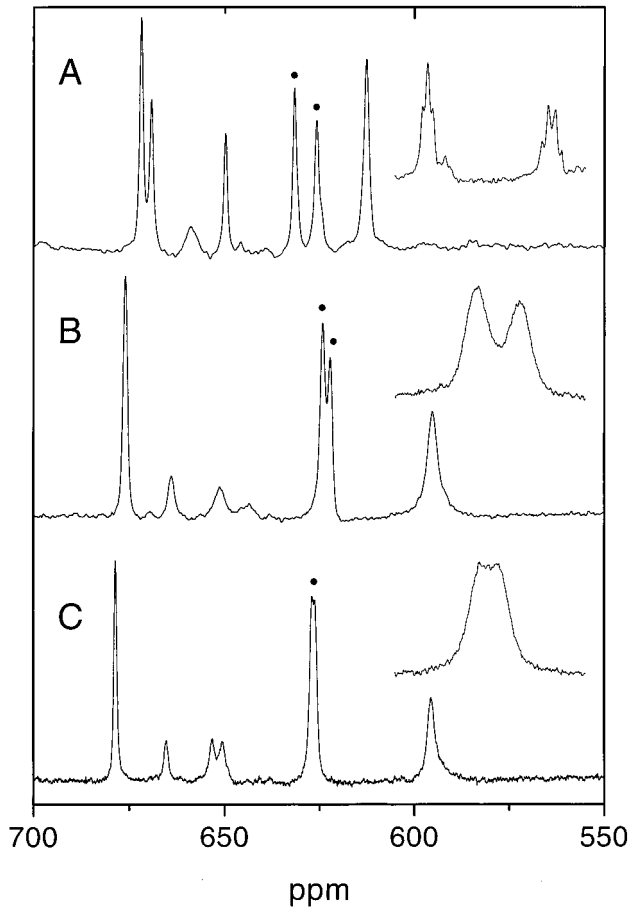

FIGURE 3: ^{113}Cd NMR spectra at 133 MHz of (A) rabbit liver ^{113}Cd$_7$-MT-2a and (B) ^{113}Cd$_7$-GIF at 298 K, and of (C) ^{113}Cd$_7$-GIF at 323 K. Conditions: 2 mM protein sample in 25 mM Tris/HCl, 50 mM NaCl at pH 8.0; 20 Hz line broadening. (Inset) Expansion of the representative resonances (●) reveals resolved [^{113}Cd, ^{113}Cd] couplings only in panel A (line broadening 5 Hz).

Table 1: Comparison of ^{113}Cd NMR Chemical Shifts (ppm) and Apparent Line widths ($\Delta\nu_{1/2}$ in hertz)[a] of the ^{113}Cd Resonances for Rabbit Liver ^{113}Cd$_7$-MT-2A and Human ^{113}Cd$_7$-GIF at 133 MHz and Different Temperatures in 25 mM Tris/HCl and 50 mM NaCl at pH 8.0

^{113}Cd$_7$-MT-2a[b]		^{113}Cd$_7$-GIF (133 MHz)				^{113}Cd$_7$-GIF (66 MHz)	
298 K		298 K		323 K		298 K	
ppm	$\Delta\nu_{1/2}$	ppm	$\Delta\nu_{1/2}$	ppm	$\Delta\nu_{1/2}$	ppm	$\Delta\nu_{1/2}$
672	81	676	154	678	113	676	81
669	81	664	225	665	155	665	91
658	180	651	360	653	242	651	131
650	74	644	140	650	268	644	120
632	77	624	194	627	(272)[c]	624	(211)[c]
626	75	622	191	626	(272)[c]	623	(211)[c]
613	130	595	338	596	265	596	137

[a] The line widths were measured at half-height of the multiplets since the deconvolution into the multiplet components was not possible. [b] Rabbit ^{113}Cd$_7$-MT-2a was remeasured for this study. [c] Apparent line width of the unresolved signals at 627/626 ppm and 624/623 ppm.

Cd(II) ions are coordinated by both bridging and terminal thiolate ligands (Table 1). However, compared with mammalian MTs, the 595 ppm resonance appears to be about 20 ppm high field shifted.

At 133 MHz, the ^{113}Cd resonances of ^{113}Cd$_7$-GIF reveal a number of striking features. Thus, there are no resolved homonuclear [^{113}Cd-^{113}Cd] couplings discerned (Figure 3, panels B and C), and all resonances show a large apparent line widths, when compared with the signals obtained for ^{113}Cd$_7$-MT-2a (Table 1). A similar trend was also seen in the corresponding ^{113}Cd NMR spectrum of ^{113}Cd$_7$-GIF acquired at 66 MHz. However, in this case, the line widths are decreased (Table 1) and for the intense resonances, a partially resolved fine structure due to homonuclear couplings was detected (data not shown). For these resonances, the observed differences in the spectra obtained at two different magnetic fields are due mainly to the contribution to transverse relaxation (T_2) by CSA, i.e., to signal line widths. The feature described above increases with the square root of the magnetic field.

In addition, the ^{113}Cd resonances of ^{113}Cd$_7$-GIF at 664, 651, and 644 ppm show a markedly reduced intensity (∼20%) and even substantially more increased line widths (at 133 MHz), when compared with the four major ^{113}Cd resonances (Figure 3, Table 1). Since almost identical spectra of ^{113}Cd$_7$-GIF were obtained using repetition rates of 0.4 and 2 s, a partial saturation of these resonances due to long T_1 relaxation values can be ruled out. In the previous ^{113}Cd NMR studies of dimeric Cd-MT, the absence of ^{113}Cd resonances of the original 3-metal cluster and a substantial broadening of the resonances of the Cd$_4$-cluster were observed (*40*). Although a small amount of dimers could be detected by gel filtration in the GIF sample after the NMR measurement (<15%), this protein aggregation cannot account for the observed NMR features. Therefore, the presence of chemical exchange processes in ^{113}Cd$_7$-GIF was also studied by investigating the temperature dependence of the ^{113}Cd NMR spectrum. Rising the temperature from 298 to 323 K resulted in a sharpening of all resonances due mainly to the decreased correlation time, τ_c (Figure 3). Remarkably, the integrals of the three minor resonances at both temperatures remained the same (∼20% of the major ones), suggesting that the major part of the signal intensities still remained undetected.

In a number of previous NMR studies, the metal organization in Cd-MT from various species has been obtained from [^{113}Cd, ^{113}Cd] COSY experiments. Despite the absence of resolved homonuclear [^{113}Cd, ^{113}Cd] couplings in ^{113}Cd$_7$-GIF, attempts to obtain at least some structural information using this type of experiments were performed at 66 MHz. However, no cross-peaks in the [^{113}Cd, ^{113}Cd] COSY spectra were detected. Double-quantum spectroscopy (2Q-COSY) is advantageous to detect frequencies of exchange-broadened, coupled spins in the indirect dimension (*41*). However, this approach requires that the coupling partners still display reasonably sharp lines. The large broadening of ^{113}Cd signals in ^{113}Cd$_7$-GIF precluded their studies by this method.

DISCUSSION

The ^{113}Cd NMR chemical shifts of ^{113}Cd$_7$-GIF are very similar to those of mammalian ^{113}Cd$_7$-MTs (*35*−*38*), suggesting that the seven Cd(II) ions in GIF form cluster structure(s) involving all 20 cysteine thiolates. This conclusion is in agreement with the results from electronic absorption and CD studies on Cd$_7$-GIF. Unfortunately, due to the absence of cross-peaks in [^{113}Cd, ^{113}Cd] COSY, the cluster localization and their topology cannot be determined. However, an assignment regarding the cluster localization

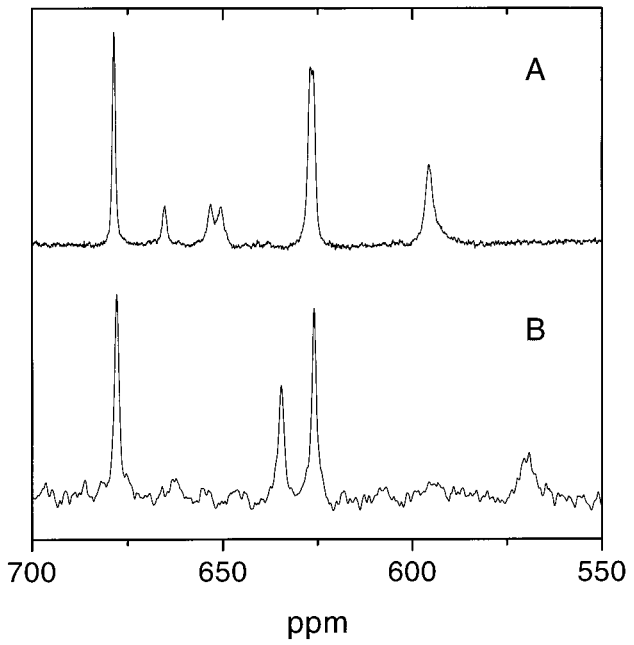

FIGURE 4: 133 MHz ^{113}Cd NMR spectra of (A) $^{113}Cd_7$-GIF and (B) $^{113}Cd_4$-GIF(32−68) (*23*) at 323 K. Conditions: 2 mM protein sample in 25 mM Tris/HCl and 50 mM NaCl at pH 8.0. Note that the chemical shifts for $^{113}Cd_4$-GIF(32−68) have been corrected for the temperature shift of the standard at 323 K.

can be made when results from our previous ^{113}Cd NMR studies on $^{113}Cd_4$-GIF(32−68) are taken into account. In this case, the ^{113}Cd NMR spectrum of $^{113}Cd_4$-GIF(32−68) at 323 K revealed four ^{113}Cd resonances at 678, 634, 628, and a broad and weak resonance at 570 ppm (Figure 4B) (*23*). By comparison of this spectrum with the $^{113}Cd_7$-GIF spectrum at 323 K, the four intense resonances at 678, 627, 626, and 596 ppm in $^{113}Cd_7$-GIF can be assigned to a Cd_4-cluster located in the C-terminal α-domain (Figure 4). Consequently, the remaining three minor ^{113}Cd resonances would correspond to a metal cluster in the N-terminal *β*-domain. Taken together the results are consistent with a similar metal distribution in both GIF and mammalian MTs. However, the 595 ppm signal at 293 K is about 20 ppm high field shifted compared to the published range of ^{113}Cd resonances insofar studied mammalian MTs. The increased shielding of this resonance suggests a coordination environment, which differs from that found in mammalian MTs. In $^{113}Cd_4$-GIF(32−68), the resonance at 570 ppm is detectable only at elevated temperature (323 K). Such a very strong temperature dependence, due most likely to fast chemical exchange processes, is absent in $^{113}Cd_7$-GIF for the corresponding 596 ppm resonance (Figure 3). The different NMR properties of this site in both species suggest that the corresponding metal-binding site is located at the linkage region between both protein domains.

The presence of a two domain structure in human Me^{II}_7-GIF allows a comparison of the spectra of the entire protein with those of its two individual domains (Figures 1 and 2) (*22*, *23*). In the electronic absorption spectra of the Cd- and Zn-containing forms, the mathematical sum of the two individual domain spectra is closely similar to the absorption spectra of the entire Cd_7- and Zn_7-GIF forms, respectively (Figures 1 and 2). Since the absorption spectra above 220 nm are dominated by the LMCT transitions, the close correspondence of these spectra implies that all 20 cysteine thiolates are involved in metal binding. However, a comparison of the corresponding CD spectra, which are highly sensitive toward structural changes, shows marked differences between the mathematical sum of the individual domains and the entire protein for both, the Cd- and Zn-forms. (Figures 1 and 2). This indicates that the two protein domains are not independent from each other. From the sum of component CD spectra alone one cannot conclude whether the structural changes are due to just one protein domain or both. However, a comparison of the ^{113}Cd NMR spectra of $^{113}Cd_3$-GIF(1−32), $^{113}Cd_4$-GIF(32−68), and $^{113}Cd_7$-GIF suggest structural alterations of both domains. Thus, the $^{113}Cd_4$-GIF(32−68) domain shows only three major ^{113}Cd resonances at 298 K, the fourth ^{113}Cd resonance at 570 ppm appears as a very broad signal only upon rising the temperature to 323 K. This behavior has been attributed to a conformational flexibility of the α-domain (*23*). Moreover, due to similar processes, no ^{113}Cd resonances have been detected for $^{113}Cd_3$-GIF(1−32) (*22*). Thus, the structures of both separated domains are significantly more flexible than in the entire protein. Consequently, a mutual structural stabilization of the α- and *β*-domains in GIF exits. This finding rises the question why the Zn_3-GIF(1−32) domain exhibits about the same growth inhibitory activity as Zn_7-GIF (*20*). We attribute this effect to an induced fit type of interaction with another factor(s) or receptor.

In view of the mutual domain interaction in GIF, the question arises regarding the presence of such effects in MTs. In mammalian Cd_7-MTs, only the isolated α-domains (residues 30−61) from rat and human liver have been studied by ^{113}Cd NMR. In these studies, no NMR evidence for dynamic processes has been obtained for the $^{113}Cd_4$-cluster. However, in the corresponding $^{113}Cd_7$-MT spectra, substantial changes in the chemical shift position of the most shielded resonance (resonance 7) compared to that in the isolated $^{113}Cd_4$-cluster from both species have also been detected (*42*, *43*). The three-dimensional structures of Me^{II}_7-MTs reveal the presence of $Me^{II}_3S_9$- and $Me^{II}_4S_{11}$-clusters in which each metal-binding site is tetrahedrally coordinated by cysteine ligands (*35*−*39*, *44*). In these structures, the affected metal-binding site in the $^{113}Cd_4S_{11}$ cluster is coordinated by cysteines occurring predominantly at the interface of both protein domains, i.e., Cys 34, 36, 37, and 50. These features together with the finding that in the Co(II) reconstituted Co_4-α-domain of MT from rabbit liver one octahedral site occurs, in addition to the three tetrahedrally coordinated sites (*45*), suggest that a mutual domain interaction also takes place in mammalin MTs.

The most striking differences between GIF and mammalian MTs are revealed by their ^{113}Cd NMR spectra at 133 MHz. In contrast to the representative $^{113}Cd_7$-MT spectrum from rabbit liver, no homonuclear [^{113}Cd, ^{113}Cd] couplings can be found in $^{113}Cd_7$-GIF spectra due to a substantially increased apparent line width of all resonances. (Figure 3, Table 1). Broadening of signals of the α- and *β*-domains due to CSA should be roughly similar for MTs and GIF and thus cannot account for the observed large line widths. This and the absence of substantial GIF aggregation suggest that

other reason(s) have to be responsible for the marked differences in both ^{113}Cd NMR spectra.

It is well established that a considerable degree of dynamic structural disorder exists in the spatial structure of Me^{II}_7-MTs (*44*, *46*). The presence of metal−thiolate cluster dynamics in Zn_7-MT has been supported by the observation of the second-shell Zn···Zn backscaterring in Zn K-edge EXAFS only upon temperature decrease to 77 K (*47*). These and other features of the metal−thiolate clusters have been interpreted in terms of cluster fluctuations (*48*). We suggest that such cluster dynamics take place in GIF in the fast-exchange regime and that the observed large line widths for all ^{113}Cd resonances reflects a weighted average of the chemical shifts of different cluster substates. These conformational cluster substates can be visualized as being structurally closely similar with metal-sites possessing a slightly altered metal coordination geometry. In general, the coalescence temperature for such an exchange process depends on both the exchange rate and the separation of the exchanging resonances (in hertz). Moreover, in the fast-exchange regime, the NMR spectra at higher field display broader lines. Indeed, in contrast to the NMR spectra of $^{113}Cd_7$-GIF acquired at 133 MHz, the observation of decreased transverse relaxation (T_2) at 66 MHz would be in agreement with such a process. Unfortunately, since the CSA is proportional to the square root of the static magnetic field, it is difficult to estimate its contribution to the overall reduced line widths at the lower magnetic field. Nevertheless, these results clearly explain the absence of cross-peaks in [^{113}Cd, ^{113}Cd] COSY.

In addition to the large line broadening, observed for all resonances of $^{113}Cd_7$-GIF, the three ^{113}Cd resonances of the three-metal cluster are low in intensity compared not only to the four-metal cluster resonances in GIF but also to the three-metal cluster resonances in mammalian MTs. Since metal loss, protein aggregation, or signal saturation could be ruled out (see above), this observation suggests that they represent only a minor NMR detectable population of this cluster. However, in the absence of additional ^{113}Cd resonances the already discussed cluster dynamics do not account for their low and temperature-independent intensity. The only explanation for this effect would be that the majority of the resonances of this cluster are exchange-broadened beyond detection.

Apart from the above-discussed local dynamics, the inorganic adamantane-like metal−thiolate clusters with the general formula $[M_4(SPh)_{10}]^{2-}$ (M = Cd^{II}, Zn^{II}, Co^{II}, and Fe^{II}) show also more profound structural fluctuations, involving temporarily breaking and reforming of the metal−thiolate bonds. This process gives rise to a number of interchanging configurational cluster substates of comparable stability (*49*). In MTs, the buried metal−thiolate clusters show a substantial kinetic lability reflected by a facile inter- and/or intramolecular metal exchange (*50*, *51*). Although the mechanism underlying this process is not yet understood, a rapid metalation and demetalation of the thiolate ligands must be accompanied by substantial changes in the tertiary structure of the protein. We propose, therefore, that two dynamic processes, which are coupled with each other and act on very different NMR time scales, influence the ^{113}Cd signals of the β-domain: (i) fast-exchange processes among different *conformational* cluster substates, accounting for the broad detectable resonances, and (ii) very slow (on the NMR time scale) *configurational* cluster fluctuations brought about by temporarily breaking and reforming of the metal−thiolate bonds. At present, the exact nature of the exchange processes cannot be derived from the experimental data. However, to illustrate the influence of the coupled slow and fast-exchange processes on the resonance of a single Cd site in the β-cluster, a schematic sketch is presented in Figure 5. Therein, the resonance at ν_a (Figure 5A) is split into two (or possibly even more) resonances at ν_b and ν_c by the slow configurational cluster rearrangements (Figure 5B). The newly established resonances at ν_b and ν_c are broadened further by exchange among the different conformational cluster substates (Figure 5C). In this process, the resonance at ν_c escapes detection by NMR due either to an extensive exchange broadening and/or to the low population of various cluster substates, considering the moderate signal/noise ratio of the spectra.

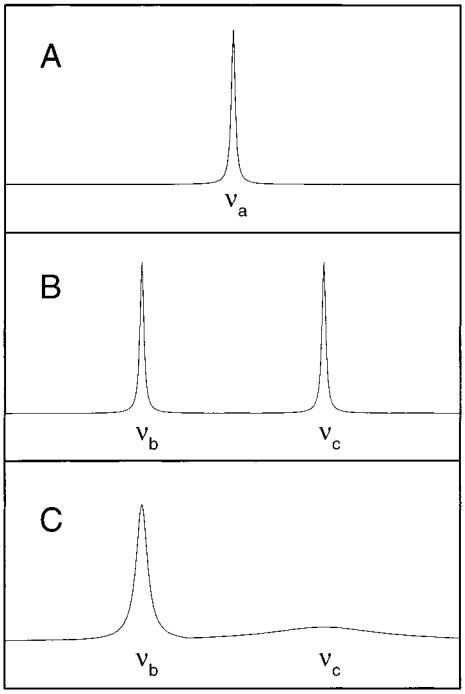

FIGURE 5: Schematic illustration of the effect of slow configurational and fast conformational fluctuations on a single ^{113}Cd site of the β-cluster in $^{113}Cd_7$-GIF (for details, see text).

Thus, it would appear that in the β-domain only one configurational cluster substate is detectable, most likely the cyclohexane-like cluster found in mammalian Cd_7-MTs. Interestingly, the detectable and the not detectable cluster resonances cannot be in fast exchange on the ^{113}Cd NMR time scale, since all nuclei bound to these sites should contribute to signal intensities otherwise. To account for this effect, the energy barrier between the detectable and not detectable configurational substate(s) should be relatively high. In this connection, it may be noted that the absence of ^{113}Cd resonances due to chemical exchange has been reported in a number of ^{113}Cd NMR studies of Cd-substituted metalloproteins (*52*, *53*). An independent support for the existence of a structurally different cluster form in the β-domain of GIF has been provided by our recent K-edge EXAFS studies of Zn_7-GIF and Zn_3-GIF(1−32), in which an outer shell backscattering of a Zn atom at about 3.28 Å was found (*19*). Such a short Zn···Zn distance is not

consistent with the cyclohexane-like $Zn_3(CysS)_9$ cluster found in mammalian MTs, where the distance is about 3.8 Å (*44*). However, a similar Zn···Zn distance of 3.16 Å has been determined by EXAFS for a binuclear $Zn_2(CysS)_6$ cluster in transcriptional activator PPR1. In this cluster, both Zn(II) ions are bridged by two CysS ligands (*54*). The proposed EXAFS model for the Zn_3-cluster in GIF shows a binuclear cluster similar to that in PPR1, which is linked with a third tetrahedral tetrathiolate Zn-site (*19*). To generate such a cluster from the cyclohexane-like $Me^{II}_3S_9$ cluster in MTs, only two cysteine residues would have to be rearranged.

In conclusion, the presented studies showed that the changes in the primary structure of GIF, when compared with mammalian MTs, result in a substantially increased flexibility of both protein domains. In view of the biological function of GIF, the presence of an overall flexible structure would be desirable for receptor and/or protein recognition or for facilitating metal exchange/transport. The studies also provide the evidence for the presence of interchanging cluster structures in the biologically active β-domain of GIF. Such cluster fluctuations must be accompanied by substantial changes of the surface topology of this domain. However, at present, it is not clear which structural form of this domain is responsible for its biological activity. In this context, it may be noted that the presented studies focused on GIF forms binding divalent metal ions. However, isolated GIF contains two homonuclear Cu(I)- and Zn(II)-clusters. Although their localization is currently unknown, it is conceivable that due to the predominantly trigonal Cu(I) coordination in native Cu,Zn-GIF (*19*), its binding to either domain may have a substantial effect on the overall protein structure and hence on the biological activity. It may be noted, moreover, that GIF expressed in a zinc containing *E. coli* culture exhibited a lower biological activity compared to isolated Cu,Zn-GIF (*11*). Thus, a deeper insight into the structural features of GIF is necessary to comprehend how the growth inhibitory activity is fulfilled. Such studies are currently in progress in our laboratory.

ACKNOWLEDGMENT

The authors would like to thank Prof. G. Roesijadi for introducing us to *E. coli* expression and Mrs. J. Eggenberger, Ch. Berger, and S. Weber-Bornhauser for valuable suggestions regarding the *E. coli* expression system. We thank also N. Walch and M. Binder for recording the NMR spectra and Dr. P. Gehrig for obtaining the ESI-MS spectra.

REFERENCES

1. Selkoe, D. J. (1991) *Neuron 6*, 487−498.
2. Uchida, Y., Ihara, Y., and Tomonga, M. (1988) *Biochem. Biophys. Res. Commun. 150*, 1263−1267.
3. Uchida, Y., Takio, K., Titani, K., Ihara, Y., and Tomonaga, M. (1991) *Neuron 7*, 337−347.
4. Erickson, J. C., Sewell, A. K., Jensen, L. T., Winge, D. R., and Palmiter, R. D. (1994) *Brain Res. 649*, 297−304.
5. Arai, Y., Uchida, Y., and Takashima, S. (1997) *Pediatr. Neurol. 17*, 134−138.
6. Palmiter, R. D., Findley, S. D., Whitmore, T. E., and Durnam, D. M. (1992) *Proc. Natl. Acad. Sci. U.S.A. 89*, 6333−6337.
7. Pountney, D. L., Fundel, S. M., Faller, P., Birchler, N. E., Hunziker, P., and Vašák, M. (1994) *FEBS Lett. 345*, 193−197.
8. Kobayashi, H., Uchida, Y., Ihara, Y., Nakajima, K., Kohsaka, S., Miyatake, T., and Tsuji S. (1993) *Mol. Brain Res. 19*, 188−194.
9. Chen, C. F., Wang, S. H., and Lin, L. Y. (1996) *Comp. Biochem. Physiol. 115B*, 27−32.
10. Kojima, S., Shimada, A., Kodan, A., Kobayashi, K., Morita, T., Yamano, Y., and Umemura, T. (1998) *Can. J. Vet. Res. 62*, 148−151.
11. Tsuji, S., Kobayashi, H., Uchida, Y., Ihara, Y., and Miyatake, T. (1992) *EMBO J. 11*, 4843−4850.
12. Kägi, J. H. R. (1993) in *Metallothioneins III* (Suzuki, K. T., Imura, N., and Kimura, M., Eds.) pp 29−56, Birkhäuser Verlag, Basel.
13. Templeton, D. M., and Cherian, M. G. (1991) *Methods Enzymol. 205*, 11−24.
14. Maret, W., and Vallee, B. L. (1998) *Proc. Natl. Acad. Sci. U.S.A. 95*, 3478−3482.
15. Moffatt P., and Seguin, C. (1998) *DNA Cell Biol. 17*, 501−10.
16. Quaife, C. J., Kelly, E. J., Masters, B. A., Brinster, R. L., and Palmiter, R. D. (1998) *Toxicol. Appl. Pharmacol. 148*, 148−157.
17. Bruinink, A., Faller, P., Sidler, C., Bogumil, R., and Vašák, M. (1998) *Chem. Biol. Interact. 115*, 167−174.
18. Bogumil, R., Faller, P., Pountney, D. L., and Vašák, M. (1996) *Eur. J. Biochem. 238*, 698−705.
19. Bogumil, R., Faller, P., Binz, P.-A., Vašák, M., Charnock, J. M., and Garner, C. D. (1998) *Eur. J. Biochem. 255*, 172−177.
20. Sewell, A. K., Jensen, L. T., Erikson, J. C., Palmiter, R. D., and Winge, D. R. (1995) *Biochemistry 34*, 4740−4747.
21. Uchida, Y., and Ihara, Y. (1995) *J. Biol. Chem. 270*, 3365−3369.
22. Faller P., and Vašák, M. (1997) *Biochemistry 36*, 13341−13348.
23. Hasler, D. W., Faller, P., and Vašák M. (1998) *Biochemistry 37*, 14966−14973.
24. Braun W., Vašák, M., Robbins, A. H., Stout, C. D., Wagner, G., Kägi, J. H. R., and Wüthrich, K. (1992) *Proc. Natl. Acad. Sci. U.S.A. 89*, 10124−10128.
25. Kosower, N. S., and Kosower, E. M., (1987) *Methods Enzymol. 143*, 76−84.
26. Laemmli, U. K. (1970) *Nature 227*, 680−685.
27. Vašák, M. (1991) *Methods Enzymol. 205*, 452−458.
28. Pedersen, A. O., and Jacobsen, J. (1980) *Eur. J. Biochem. 106*, 291−295.
29. Marston, A. O. (1986) *Biochem. J. 240*, 1−12.
30. Vašák, M., and Kägi, J. H. R. (1983) in *Metal Ions in Biol. Syst.* (Sigel, H., Ed.) Vol. 15, pp 213−275, Marcel Dekker Inc., New York.
31. Vašák, M., Kägi, J. H. R., and Hill, H. O. A. (1981) *Biochemistry 20*, 2852−2856.
32. Henehan, C. J., Pountney, D. L., Zerbe O., and Vašák, M. (1993) *Protein Sci. 2*, 1756−1764.
33. Willner, H., Vašák, M., and Kägi, J. H. R. (1987) *Biochemistry 26*, 6287−6292.
34. Wüthrich, K. (1991) *Methods Enzymol. 205*, 502−520.
35. Arseniev, A., Schultze, P., Wörgötter, E., Braun, W., Wagner, G., Vašák, M., Kägi, J. H. R., and Wüthrich, K. (1988) *J. Mol. Biol. 201*, 637−657.
36. Frey M. H., Wagner, G., Vašák, M., Sørensen, O. W., Neuhaus, D., Wörgötter, E., Kägi, J. H. R., Ernst, R. R., and Wüthrich, K. (1985) *J. Am. Chem. Soc. 107*, 6847−6851.
37. Otvos J. D., and Armitage, I. M. (1980) *Proc. Natl. Acad. Sci. U.S.A. 77*, 7094−7098.
38. Schultze, P., Wörgötter, E., Braun, W., Wagner, G., Vašák, M., Kägi, J. H. R., and Wüthrich, K., (1988) *J. Mol. Biol. 203*, 251−268.
39. Messerle, B. A., Schäffer, A., Vašák, M., Kägi, J. H. R., and Wüthrich, K. (1990) *J. Mol. Biol. 214*, 765−779.
40. Palumaa, P., Mackay, E. A., and Vašák, M. (1992) *Biochemistry 31*, 2181−2186.
41. Rance, M., Chazin, W. J., Dalvit, C., and Wright, P. E., (1989) *Methods Enzymol. 176*, 114−134.

42. Boulanger Y., Armitage, I. M., Miklossy, K. A., and Winge D. R. (1982) *J. Biol. Chem. 257*, 13717−13719.
43. Kull, F. J., Reed, M. F., Elgren, T. E., Ciardelli, T. L., and Wilcox, D. E. (1990) *J. Am. Chem. Soc. 112*, 2291−2298.
44. Robbins, A. H., McRee, D. E., Williamson, M., Collett, S. A., Xuong, N. H., Furey, W. F., Wang, B. C., and Stout, C. D (1991) *J. Mol. Biol. 221*, 1269−1293.
45. Good, M., and Vašák, M. (1986) *Biochemistry 25*, 3328−3334.
46. Messerle, B. A., Bos, M., Schäffer, A., Vašák, M., Kägi, J. H. R., and Wüthrich, K. (1990) *J. Mol. Biol. 214*, 781−786.
47. Abrahams, I. L., Bremner, I., Diakun, G. P., Garner, C. D., Hasnain, S. S., Ross, I., and Vašák, M. (1996) *Biochem. J. 236*, 585−589.
48. Vašák, M. (1986) *Environ. Health Persp. 65*, 193−197.
49. Hagen, K. S., Stephan, D. W., and Holm, R. H. (1982) *Inorg. Chem. 21*, 3928−3936.
50. Nettesheim, D. G., Engeseth, H. R., and Otvos, J. D. (1995) *Biochemistry 24*, 6744−6751.
51. Otvos, J. D., Liu, X., Li, H., Shen, G., and Basti, M. (1993) in *Metallothionein III* (Suzuki, K. T., Kimura, M., and Imura, N., Eds.) pp 29−56, Birkhäuser Verlag, Basel.
52. Coleman, J. E., Armitage, I. M., Chlebovski, J. F., Otvos, J. D., and Uiterkamp, A. J. (1979) in *Biological application of magnetic resonance* (Schulman, R. G., Ed.) pp 345−395, Academic press, New York.
53. Gettins, P., and Coleman, J. E. (1983) *J. Biol. Chem. 258*, 396−407.
54. Ball, L. J., Diakun, G. P., Gadhavi, P. L., Young, N. A., Armstrong, E. M., Garner, C. D. and Laue, E. D. (1995) *FEBS Lett. 358*, 278−282.

BI990489C